Equation of State and Miscibility Behavior of Compressible Binary Lattice Polymers. A Monte Carlo Study and Comparison with Partition Function Theories

Peter Cifra

Polymer Institute, Slovak Academy of Sciences, 842 36 Bratislava, Slovakia

Erik Nies* and Jabik Broersma

Eindhoven Polymer Laboratories, Faculty of Chemical Engineering, Eindhoven University of Technology, P.O. Box 513, 5600MB Eindhoven, The Netherlands

Received January 30, 1996; Revised Manuscript Received May 28, 1996[⊗]

ABSTRACT: In a continuing study on the properties of the compressible lattice model, the equation of state and miscibility behavior of binary mixtures of lattice chains is explored. Monte Carlo simulations are performed in the NpT and semi-grand-canonical μpT ensemble for varying compositions and several combinations of the three interactional parameters characterizing the binary mixture. In all simulations the chain lengths of both components are taken to be equal. In addition to the thermodynamic information, microscopic information on the number of different contacts and the mean square end-to-end distance is collected, too. The Monte Carlo results are used to examine the predictions of lattice model theories derived from statistical mechanics. To this purpose the nonrandom mixing theory for the binary compressible mixture, based on the quasi-chemical approximation of Guggenheim, is presented. The theory is compared in detail to the collected simulation data. Although the theory is completely general, the comparison is limited, by the simulation data, to symmetric chain lengths. Furthermore, the relation of this theory to other frequently used approximate theories is explained. It is shown that the nonrandom mixing theory gives the best agreement with simulation data. Nevertheless, for the miscibility behavior and the number of contacts in particular, deviations remain that are related to neglect of the excluded volume of the chain molecules and critical phenomena.

1. Introduction

The lattice model has been the subject of numerous publications. This interest in the lattice model in polymer science stems from the pioneering work of Staverman,[1,2] Flory,[3,4] and Huggins[5,6] (SFH) from more than half a century ago. They independently showed that theories based on the lattice model were capable of capturing the main features of the UCST miscibility behavior of polymer solutions. (A mixture possesses a UCST miscibility gap if an initially homogeneous solution demixes in two liquid phases upon cooling. In a binary mixture the top of this coexistence curve is the (UCST) critical point. If demixing occurs upon heating a homogeneous solution, the miscibility gap has a minimum. Again, in the case of a binary mixture this minimum is the LCST critical point). The results of these authors set the standard for much theoretical and experimental investigations of the thermodynamic properties, in particular the phase behavior of polymer solutions and blends.

Later, it was realized that the original Staverman−Flory−Huggins (SFH) theory did not provide a theoretical foundation for the frequently occurring LCST phase behavior. The inadequacy of the original SFH theory was remedied by several authors along many different lines. It was found that one possible cause for the LCST miscibility is a difference in the compressibility of the mixture constituents.[7] One simple and appealing way to model compressibility is the introduction of vacancies on the lattice. In addition, the lattice model with vacancies makes applications to the equation of state of pure components and mixtures possible.[8−10]

Initially, these theoretical predictions could only be compared to experimental data and the identification of the causes for the deviations between theory and experiment was not always straightforward. With the advent of computer simulations, it has also become feasible to compare theoretical predictions and simulations for the same model. In the framework of statistical mechanics,[11] and properly accounting for finite size effects,[12] simulations essentially provide the true properties of the model. Hence, by comparing theory and simulation, it is possible to verify, of falsify, certain theoretical approximations that are inevitable in arriving at (attractive) theoretical expressions for any nontrivial model.

It should be mentioned that the lattice model is not at all an adequate model for the liquid state. In effect, these inadequacies can be nicely demonstrated by confronting off-lattice simulations with the theoretical predictions of the lattice model. Subsequently, hybrid theories, combining lattice and off-lattice aspects, were proposed to alleviate the deficiencies of the original lattice model.[13−16] It should be pointed out that these deficiencies were already recognized much earlier and were also removed along different lines in cell theories (developed by Lennard-Jones and Devonshire for monatomics[17] and extended to polymers by Prigogine[18]) and in hole theories (systematically investigated in the study of the equation of state properties of polymer systems by Simha and co-workers[19,20] and systematically improved and applied to miscibility behavior of solutions and blends more recently.[21−24]) Notwithstanding the success of these alternative theories in the description and prediction of thermodynamic properties of real liquid polymers and the important drawbacks of the original lattice model, the study of the latter can still contribute to the understanding of theories. For instance, the lattice model can serve as a test field to investigate existing theories and to devise and test new

[⊗] Abstract published in *Advance ACS Abstracts,* August 15, 1996.

S0024-9297(96)00154-4 CCC: $12.00

Table 1. Summary of Useful Variables

segment fraction of component I (I = A,B)	$\phi_I = \frac{N_I s_I}{N_A s_A + N_B s_B}$
occupied site fraction	$y = \frac{N_A s_A + N_B s_B}{N_A s_A + N_B s_B + N_h}$ $\gamma = 2/z$ $\alpha_I = \gamma(1 - 1/s_I)$ $\alpha = \alpha_A\phi_A + \alpha_B\phi_B$
number-average chain length	$s = \frac{N_A s_A + N_B s_B}{N_A + N_B}$
total number of pairs of contact sites	$Q = (N_A s_A(1 - \alpha_A) + N_B s_B(1 - \alpha_B) + N_h)/\gamma$
contact site fraction of component I	$u_I = \frac{N_I(s_I(z-2)+2)}{2Q} = \frac{(1-\alpha_I)\phi_I y}{1-\alpha y}$
contact site fraction of A and B	$u = u_A + u_B = \frac{(1-\alpha)y}{1-\alpha y}$
contact site fraction of vacancies	$u_h = \frac{zN_h}{2Q} = \frac{1-y}{1-\alpha y}$
contact segment fraction of component I	$\theta_I = \frac{(1-\alpha_I)\phi_I}{1-\alpha}$

theoretical approximations. For this purpose, three advantages can be noted: (i) the same model can easily be applied in theory and simulation (in a continuum, one frequently has to resort to differences in the model for theory and simulation), (ii) lattice simulations are more efficient than off-lattice simulations and can even be performed for densities typical of a polymer melt, and (iii) the derivation of theoretical approximations for the lattice model is easier than for an off-lattice model in most cases.

One of the first systematic comparisons of theory and simulation for the simple lattice model was performed and discussed in a series of papers by Sariban and Binder.[25−27] These authors investigated a binary polymer mixture on a lattice with a constant fraction of vacancies.[25−27] For symmetric mixtures (chain lengths and self-interaction constants of both components are set equally and only one interaction parameter is employed to characterize the system) the liquid−liquid coexistence curve was investigated as a function of chain length, temperature, and vacancy fraction. As the vacancy fraction was fixed, the simulations do not really represent a binary compressible mixture and are more appropriately discussed as a ternary mixture of vacancies and two chainlike components. The authors showed that the so-called quasi-chemical approximation of Guggenheim is a significant improvement over the Staverman−Flory−Huggins theory. Although they only compared to the incompressible quasi-chemical theory, derived for a completely packed lattice, the sucess of the quasi-chemical approach was attributed to a refined evaluation of the external contacts the chain molecules can make. The simulations were extended to asymmetrical ternary mixtures with asymmetries in the interactional constants by Deutsch[28] and to asymmetrical chain lengths by Mueller and Binder,[29] using so-called reweighting or histogram extrapolation techniques.

In addition, the equation of state of single components has been investigated by different authors. Initially for athermal conditions[30] and subsequently for systems including attractive interaction energies,[10,31] it was shown in accordance with the previous findings that the NRM theory was far better than the SFH theory. In contrast to the situation for single components, simulation studies on the equation of state of mixtures are not available, apart from a single study by Mueller and Binder[29] for the bond fluctuating model.[32]

Table 2. Summary of Different Types of Contact and the Corresponding Contact Energies

kind of contact	number of contact pairs	interaction constant
AA	$Q(u_A - X_{AB} - X_{Ah})$	$-\epsilon_{AA}$
BB	$Q(u_B - X_{AB} - X_{Bh})$	$-\epsilon_{BB}$
hh	$Q(u_h - X_{Ah} - X_{Bh})$	$-\epsilon_{hh} = 0$
AB	QX_{AB}	$-\epsilon_{AB}$
Ah	QX_{Ah}	$-\epsilon_{Ah} = 0$
Bh	QX_{Bh}	$-\epsilon_{Bh} = 0$

In the present contribution, the properties of compressible binary polymer mixtures on a lattice were investigated. The equation of state of mixtures with varying composition and different combinations of self- and cross-interactional constants was investigated. Due to the compressibility, the self-interaction energy parameters directly influence the properties of mixture, this in contrast to the incompressible system. Furthermore, the liquid−liquid binodal coexistence of symmetric compressible polymer mixtures was studied. At the same time, the influence of pressure on this heterogeneous phase equilibrium was established. The simulation results were compared in detail with the predictions according to different theories including the nonrandom mixing theory. In the next section, the NRM theory is introduced and its relation to different approximations is presented. Subsequently, the employed simulation techniques are described. In a following section, the results are presented and discussed in conjunction with the theories. Finally, the conclusions and future work are outlined.

2. Theory

The lattice model for a binary mixture of linear chains is investigated. The mixture contains N molecules in total, N_A molecules of type A and N_B of type B. Molecules A and B occupy s_A and s_B consecutive lattice sites, respectively, on the lattice with coordination number z. Volume changes are accommodated by the presence of N_h vacancies. Hence, the total volume of the mixture is

$$V = v_0(N_A s_A + N_B s_B + N_h) \tag{1}$$

with v_0 the lattice site volume.

The variables summarized in Table 1 will be useful in the subsequent derivation and analysis. Nearest-neighbor contacts interact with a constant interaction energy, defined in Table 2. Note that the contact energy parameters are positive numbers; i.e., the sign of the energy parameters is explicitly shown. These interactions influence the mixing of molecules at the segmental level and may lead to deviations from random mixing, obtained in the athermal case. The six different types of contacts in a binary compressible mixture are uniquely determined in terms of the contact site fractions and three extra microscopic parameters, X_{AB}, X_{Ah}, and X_{Bh}.[24]

A possible route to obtain theoretical values for the thermodynamic properties of the lattice model is offered by the partition function Z[11,18]

$$Z(N_A,N_B,T,V) = \sum_{X_{AB},X_{Ah},X_{Bh}} g(N_A,N_B,T,V,X_{AB},X_{Ah},X_{Bh}) \times \exp[-E_0(N_A,N_B,T,V,X_{AB},X_{Ah},X_{Bh})/kT] \quad (2)$$

The summation on the right-hand side of eq 2 runs over all possible values of the parameters X_{AB}, X_{Ah}, and X_{Bh}. The internal energy E_0 and the available number of configurations g are functions of the indicated arguments, with T the absolute temperature and k the Boltzmann constant. For pairwise nearest-neighbor interaction constants, the internal energy is easily calculated

$$E_0 = -Q[\epsilon_{AA}(u_A - X_{AB} - X_{Ah}) + \epsilon_{BB}(u_B - X_{AB} - X_{Bh}) + 2\epsilon_{AB}X_{AB}] \quad (3)$$

The configurational factor g can only be obtained approximately. The expression proposed by Guggenheim[33] is used here

$$g = g_{HH}\frac{[(QX^*_{AB})!]^2[(QX^*_{Ah})!]^2[(QX^*_{Bh})!]^2}{[(QX_{AB})!]^2[(QX_{Ah})!]^2[(QX_{Bh})!]^2} \times \frac{[Q(u_A-X^*_{AB}-X^*_{Ah})]![Q(u_B-X^*_{AB}-X^*_{Bh})]![Q(u_h-X^*_{Ah}-X^*_{Bh})]!}{[Q(u_A-X_{AB}-X_{Ah})]![Q(u_B-X_{AB}-X_{Bh})]![Q(u_h-X_{Ah}-X_{Bh})]!} \quad (4)$$

$$\ln(g_{HH}) = \phi_A \ln(\phi_A)/s_A + \phi_B \ln(\phi_B)/s_B + \ln(y)/s + (1-y)\ln(1-y)/y - (1-\alpha y)\ln(1-\alpha y)/\gamma y \quad (5)$$

The normalizing factor g_{HH} assures that the combinatorial factor derived independently by Huggins,[6] Guggenheim,[33] and Staverman[2] is recovered in the case of random mixing. In this case, the microscopic parameters X_{AB}, X_{Ah}, and X_{Bh} obtain the values X^*_{AB}, X^*_{Ah}, and X^*_{Bh}. The remaining factors in eq 4 result if pairs of contact sites are assumed to behave as independent entities.[33] In comparison with the well-known Staverman−Flory−Huggins result, the approximation of Huggins, Guggenheim, and Staverman contains an extra contribution, given by the last term in the expression for $\ln(g_{HH})$. This correction represents the influence of the segmental connectivity typical of chain molecules. It was shown previously that this correction quite effectively accounts for the chain connectivity.[10] The exact evaluation of the full partition function, eq 2, is impossible and the quasi-chemical approximation amounts to replacing the summation by its maximum term:[33]

$$Z(N,\phi_A,T,V) = g(N,\phi_A,T,V,\bar{X}_{AB},\bar{X}_{Ah},\bar{X}_{Bh}) \times \exp[-E_0(N,\phi_A,T,V,\bar{X}_{AB},\bar{X}_{Ah},\bar{X}_{Bh})/kT] \quad (6)$$

The values $\bar{X}_{IJ}$ (IJ = AB, Ah, Bh), maximizing the partition function, are found using

$$\left.\frac{\partial Z}{\partial X_{IJ}}\right|_{T,V,\phi_A,X_{KL\neq IJ}} = 0 \quad (7)$$

The derivatives result in the following set of equations for the $\bar{X}_{IJ}$'s:

$$\bar{X}_{AB}{}^2 \exp(-(\epsilon_{AA} + \epsilon_{BB} - 2\epsilon_{AB})/kT) = (u_A - \bar{X}_{AB} - \bar{X}_{Ah})(u_B - \bar{X}_{AB} - \bar{X}_{Bh}) \quad (8a)$$

$$\bar{X}_{Ah}{}^2 \exp(-\epsilon_{AA}/kT) = (u_A - \bar{X}_{AB} - \bar{X}_{Ah})(u_h - \bar{X}_{Ah} - \bar{X}_{Bh}) \quad (8b)$$

$$\bar{X}_{Bh}{}^2 \exp(-\epsilon_{BB}/kT) = (u_B - \bar{X}_{AB} - \bar{X}_{Bh})(u_h - \bar{X}_{Ah} - \bar{X}_{Bh}) \quad (8c)$$

The solution of eqs 8 in the athermal case results in explicit relations for the X^*_{IJ}'s

$$X^*_{AB}{}^2 = u_A u_B \quad (9a)$$

$$X^*_{Ah}{}^2 = u_A u_h \quad (9b)$$

$$X^*_{Bh}{}^2 = u_B u_h \quad (9c)$$

Combining eqs 3−6 in the relation $A = -kT\ln(Z)$ results in an expression for the Helmholtz free energy:

$$A/NskT = \phi_A \ln(\phi_A)/s_A + \phi_B \ln(\phi_B)/s_B + \ln(y)/s + (1-y)\ln(1-y)/y - (1-\alpha y)\ln(1-\alpha y)/\gamma y - \frac{(1-\alpha y)}{\gamma y}[2u_A \ln(u_A) + 2u_B \ln(u_B) + 2u_h \ln(u_h) - (u_A - \bar{X}_{AB} - \bar{X}_{Ah})\ln(u_A - \bar{X}_{AB} - \bar{X}_{Ah}) - (u_B - \bar{X}_{AB} - \bar{X}_{Bh})\ln(u_B - \bar{X}_{AB} - \bar{X}_{Bh}) - (u_h - \bar{X}_{Ah} - \bar{X}_{Bh})\ln(u_h - \bar{X}_{Ah} - \bar{X}_{Bh}) - 2\bar{X}_{AB}\ln(\bar{X}_{AB}) - 2\bar{X}_{Ah}\ln(\bar{X}_{Ah}) - 2\bar{X}_{Bh}\ln(\bar{X}_{Bh})] - (1-\alpha y)\epsilon/(\gamma y kT) \quad (10)$$

$$\epsilon = \epsilon_{AA}(u_A - \bar{X}_{AB} - \bar{X}_{Ah}) + \epsilon_{BB}(u_B - \bar{X}_{AB} - \bar{X}_{Bh}) + 2\epsilon_{AB}\bar{X}_{AB} \quad (11)$$

The equation of state (EoS) of the binary mixture is related to the free energy by

$$p = -\left.\frac{\partial A}{\partial V}\right|_{N_A,N_B,T} \quad (12)$$

By straightforward algebra, this equation can be written in reduced form:

$$pv_0/kTy = -\ln(1-y)/y - 1 + 1/s + \ln(1-\alpha y)/\gamma y + \alpha/\gamma + \frac{1}{\gamma}[2u_A \ln(u_A) + 2u_B \ln(u_B) + 2u_h \ln(u_h) - (u_A - \bar{X}_{AB} - \bar{X}_{Ah})\ln(u_A - \bar{X}_{AB} - \bar{X}_{Ah}) - (u_B - \bar{X}_{AB} - \bar{X}_{Bh})\ln(u_B - \bar{X}_{AB} - \bar{X}_{Bh}) - (u_h - \bar{X}_{Ah} - \bar{X}_{Bh})\ln(u_h - \bar{X}_{Ah} - \bar{X}_{Bh}) - 2\bar{X}_{AB}\ln(\bar{X}_{AB}) - 2\bar{X}_{Ah}\ln(\bar{X}_{Ah}) - 2\bar{X}_{Bh}\ln(\bar{X}_{Bh})] - \frac{1}{\gamma y kT}(\epsilon - (\epsilon_{AA}\theta_{AA}{}^2 + \epsilon_{BB}\theta_{BB}{}^2)u) \quad (13)$$

Other thermodynamic properties can be derived from the Helmholtz free energy using standard thermodynamic relations. In the subsequent analysis, binodal and critical conditions for liquid−liquid coexistence are investigated next to the EoS. The necessary equations were accurately computed numerically using standard Fortran library routines.[34] The coexistence of two liquid phases is governed by the equality of the chemical potential of both components in the coexisting phases:[35]

$$\mu'_A = \mu''_A \quad \text{and} \quad \mu'_B = \mu''_B \quad (14)$$

The critical condition obeys the following conditions:[35]

$$\left.\frac{\partial^2 G}{\partial \phi_B^2}\right|_{p,T} = 0 \text{ and } \left.\frac{\partial^3 G}{\partial \phi_B^3}\right|_{p,T} = 0 \quad (15)$$

Equations 10 and 11 also comprise more simple theories. In a first simplification, eqs 9 are assumed to be valid (making eqs 8 obsolete) and the compressible analog of the Huggins lattice theory (HLF) is obtained. The free energy and equation of state can be reduced to

$$A/NskT = \phi_A \ln(\phi_A)/s_A + \phi_B \ln(\phi_B)/s_B + \ln(y)/s + (1-y)\ln(1-y)/y - (1-\alpha y)\ln(1-\alpha y)/\gamma y - u\epsilon/(\gamma kT) \quad (16)$$

$$pv_0/kTy = -\ln(1-y)/y - 1 + 1/s + \ln(1-\alpha y)/\gamma y + \alpha/\gamma - \frac{(1-\alpha)y\epsilon}{\gamma(1-\alpha y)^2 kT} \quad (17)$$

$$\epsilon = \epsilon_{AA}\theta_A^2 + \epsilon_{BB}\theta_B^2 + 2\epsilon_{AB}\theta_A\theta_B \quad (18)$$

In addition, while ignoring the difference between the contact segment fraction and segment fractions ($z \rightarrow \infty$; $\alpha \rightarrow 0$, but $z\epsilon$ remaining finite), the compressible Staverman−Flory−Huggins expression is recovered, which is identical to the lattice fluid theory of Sanchez and Lacombe (LF) in its most simple version.[7,8] Physically, taking the limit $z \rightarrow \infty$ amounts to ignoring the influence of covalent bonds that are not able to make external contacts.

$$A/NskT = \phi_A \ln(\phi_A)/s_A + \phi_B \ln(\phi_B)/s_B + \ln(y)/s + (1-y)\ln(1-y)/y - y\epsilon/(\gamma kT) \quad (19)$$

$$pv_0/kTy = -\ln(1-y)/y - 1 + 1/s - \frac{y\epsilon}{\gamma kT} \quad (20)$$

$$\epsilon = \epsilon_{AA}\phi_A^2 + \epsilon_{BB}\phi_B^2 + 2\epsilon_{AB}\phi_A\phi_B \quad (21)$$

An important consequence of the random mixing approximation is that the pure component parameters do not explicitly enter the equation of state. This is only done by the definition of an effective interaction energy ϵ and the average chain length s (in the case of the HLF theory, the composition-averaged parameter α enters the equations, too). This implies that a binary compressible mixture effectively displays identical behavior to a single-component fluid with properties defined as suitable averages of the constituents, which for the LF theory are given by

$$s \rightarrow s = (\phi_A/s_A + \phi_B/s_B)^{-1}$$

$$\epsilon \rightarrow \epsilon = \epsilon_{AA}\phi_A^2 + \epsilon_{BB}\phi_B^2 + 2\epsilon_{AB}\phi_A\phi_B$$

and by the following for the HLF theory:

$$s \rightarrow s = (\phi_A/s_A + \phi_B/s_B)^{-1}$$

$$\epsilon \rightarrow \epsilon = \epsilon_{AA}\theta_A^2 + \epsilon_{BB}\theta_B^2 + 2\epsilon_{AB}\theta_A\theta_B$$

$$\alpha \rightarrow \alpha = \alpha_A\phi_A + \alpha_B\phi_B$$

In the case of the full theory, which includes the effects of interactions on the mixing of pairs of segments, the pure component parameters explicitly enter the equation of state (eq 13) by virtue of eqs 8. In the comparison between theory and simulation data, use will be made of the effective component principle derived from the LF theory. Deviations from this concept both in the simulations and in the full theory will become clear in the discussion.

3. Monte Carlo Simulations

3.1. Homogeneous Mixtures. In a first type of Monte Carlo (MC) simulation, the properties of homogeneous binary mixtures are investigated as a function of interactions, composition, and pressure. This is a direct and straightforward extension of previous work on the properties of pure components. These simulations operate in the NpT ensemble, where pressure is exerted by a scanning piston.[10] The self-avoiding lattice chains of type A and B are placed on a cubic lattice, with each site being occupied once at most. Nearest-neighbor segments, which are not covalently bonded, have interaction energies depending on the type of segments as is summarized in Table 2. Mixtures of variable composition, consisting of 200−500 chains of chain length $s_A = s_B = 30$ are placed in a rectangular box between a solid wall and a moving piston, which both represent volume obstacles. In the remaining two directions, periodic boundary conditions are imposed. The rectangular box has 50 sites in the direction perpendicular to the wall and piston and 22 in the other two directions. The thermodynamic states are equilibrated by configuration moves (reptation) and volume fluctuations imposed by the piston, which scans randomly site-by-site toward or away from the wall.[10] The Metropolis sampling criterion is based on the following acceptance probability P:

$$P = \min(1, \exp(e\Delta n - p\Delta V/kT)) \quad (22a)$$

$$e\Delta n = e_{11}\Delta n_{11} + e_{22}\Delta n_{22} + e_{12}\Delta n_{12} \quad (22b)$$

$$e_{11} = \epsilon_{11}/kT,\ e_{22} = \epsilon_{22}/kT, \text{ and } e_{12} = \epsilon_{12}/kT \quad (22c)$$

where Δn_{IJ} is the change in the number of nearest-neighbor interactions with chain segments introduced by a trial move of chains and ΔV is the trial volume change always equal to the volume of a single lattice site. Both ϵ and e variables will be called interactional parameters. Although not strictly necessary, absolute units are used by choosing $T = 300$ K and the volume of 1 mol of lattice equal to $v^* = 0.0001$ m^3/mol, which closely represents the molar volume of a polystyrene segment. Employing the NpT ensemble technique, the equation of state and the different type of contacts are evaluated for mixtures with varying composition and several combinations of interactional constants. For the zero-pressure simulations, the polymer slab is condensed to the wall by applying a wall−segment interaction energy, varying with composition to mimic the average interaction of the segment in the bulk region, to avoid surface segregation.[36]

3.2. Liquid−Liquid Coexistence. In the second type of simulation, heterogeneous phase equilibria are investigated, applying the isobaric−isothermal semigrand-canonical ensemble technique. In these simulations, the pressure dependence of the liquid−liquid coexistence curve is obtained. As far as we are aware, these are the first simulations of this problem. In the most general situation, the simulation of heterogeneous phase equilibria requires two simulation boxes repre-

senting the coexisting phases.[37] The equality of chemical potential in the coexisting phases, given by eq 14, can be guaranteed by incorporating the random extraction of a component in one phase and the insertion of it in the other phase in the simulation scheme. This insertion of a chain molecule in a dense medium is extremely difficult and special simulation algorithms were developed.[38] However, these schemes are not successful in the simulation of dense polymer mixtures considered here. Fortunately, in the case of symmetric mixtures ($\epsilon_{AA} = \epsilon_{BB}$ and $s_A = s_B$), the simulation can be drastically simplified.[25−27,39] At coexistence, the chemical potential of component A and (B) is not equal in both phases, but due to the symmetry the chemical potentials of components A and B themselves are equal. Therefore, the composition of one of the coexisting phases can be determined in a single simulation box, in which the equality of chemical potential of A and B is established if allowance is made for a random exchange of a type A for B and vice versa. In this way, the problematic insertion of a chain into a condensed phase is avoided and equilibrium then represents one of the two phases of the symmetric phase equilibrium. This so-called semi-grand-canonical ensemble technique operating at constant volume was devised by Sariban and Binder.[25−27,39] In our situation, the technique was extended to constant pressure and therefore the technique was dubbed the isobaric−isothermal semi-grand-canonical ensemble technique. Just as in the simulation described in section 3.1, reptation and volume fluctuation moves were applied. In addition, a random switching of type A and B and vice versa was attempted. Those last moves had to be evaluated for changes of interactional energy in the same way as for configurational moves. The difference is that now all interactions of the chain (before and after the quality switch) are evaluated, while for reptation one has to look at the changes in interactions at the head and tail of the chain only. The quality exchange and the volume fluctuation were performed each 100 configurational moves. To avoid fluctuations in composition from one coexisting phase to the other in the simulation box, one of the components was restricted to no more than half of the total number of chains. The total number of moves used was 2×10^9, a first quarter of which was allowed for equilibration while the rest was for collecting ensemble averages, which were collected each 5000 moves. In all simulations of the liquid−liquid coexistence, 484 chains were used in the box. The interactional constants were given the values $\epsilon_{AA}/k = \epsilon_{BB}/k = 200$ K and $\epsilon_{AB}/k = 188.77542$ K. These values were chosen to give a convenient critical temperature according to the NRM theory. The composition and density of the coexisting phases were determined at several selected pressures and temperatures. Along the binodal curve for $p = 0$ bar, the end-to-end distance of both components was evaluated.

4. Discussion

4.1. Homogeneous Mixtures. In all simulations the chain lengths of both components are taken to be equal and fixed ($s_A = s_B = s = 30$). Hence, in this discussion only systems symmetric in chain lengths are being considered. However, the theory is completely general and can be easily applied to situations involving asymmetries in e.g. chain length. As a result of the chain length symmetry, the contact site fractions and segment fractions defined in Table 1 are directly proportional and the proportionality factor depends on density only:

$$u_I = \frac{(1-\alpha_I)y\phi_I}{1-\alpha y} = \frac{(1-\alpha)y}{1-\alpha y}\phi_I \tag{23}$$

Hence, the same effective interactional parameter can be used to represent the composition dependence of the data in the LF and HLF theories:

$$\epsilon_H = ((1-\alpha)y/(1-\alpha y))^2 \langle\epsilon\rangle \tag{24a}$$

$$\epsilon_{FH} = y^2\langle\epsilon\rangle \tag{24b}$$

$$\langle\epsilon\rangle = \epsilon_{AA}\phi_A{}^2 + \epsilon_{BB}\phi_B{}^2 + 2\epsilon_{AB}\phi_A\phi_B \tag{24c}$$

$$\langle e\rangle = e_{AA}\phi_A{}^2 + e_{BB}\phi_B{}^2 + 2e_{AB}\phi_A\phi_B \tag{24d}$$

Clearly, in these cases, the effects of density and blend composition are completely factored and binary mixtures can be considered as a single component with chain length s and an effective interaction parameter $\langle\epsilon\rangle$, depending on the blend composition only. It should be noted that the situation becomes slightly more complicated if the components have different chain lengths. In this case, a strict separation of composition and density is not obtained for the Huggins approximation. Consequently, the Huggins and Staverman−Flory−Huggins approximations have to be discussed separately.

In a first set of simulation data the pure component interaction parameters were set equal ($e_{AA} = e_{BB} = 0.5$) and the cross-interactional parameter was given the value $e_{AB} = 0.8$. In Figure 1 the density of mixtures with compositions ϕ_B varying between $0 < \phi_B < 0.5$ is presented as a function of the effective cross-interactional parameter $\langle e\rangle$ defined in eq 24d. It should be noted that the mixtures have negative excess volumes; i.e., a densification upon mixing with respect to the pure components occurs. The simulation data are compared to pure component results obtained previously and to the different theoretical predictions. By first considering the random mixing theories LF (···) and HLF (-·-), two conclusions can be drawn: (i) These theories predict too high a density, although the agreement between simulation and theory improves at higher density. The observed deviations between theory and simulation have been discussed in detail previously and will not be repeated here.[10] (ii) As expected, the theories obey the effective component principle and no difference between

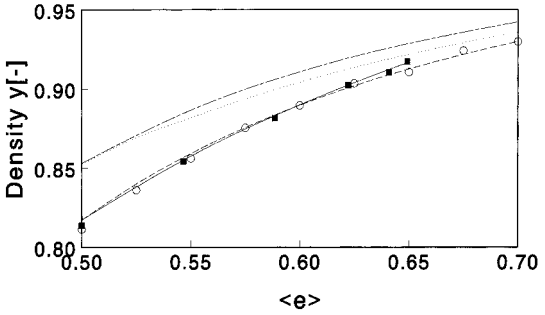

Figure 1. Density y as a function of the effective interaction parameter $\langle e\rangle$ for pure components (○) and mixtures (■) ($e_{AA} = e_{BB} = 0.5$, $e_{AB} = 0.8$, and $0 \le \phi_B \le 0.5$) representing negative excess volumes. Lines represent predictions according to different theories: LF mixture and pure component (···), HLF mixture and pure component (−·−), and NRM theory mixture (—) and pure component (− − −).

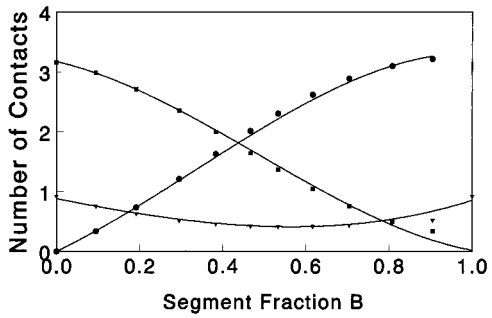

Figure 2. Number of different type of contacts as a function of composition for the parameters used in Figure 1. AA contacts (■), AB contacts (●), and Ah contacts (▼). Lines are predictions according to NRM theory.

pure components and mixtures exists. As a matter of fact, the results for the random mixing theories are identical in all the comparisons to be presented and will be omitted in subsequent figures.

It is more interesting to inspect the predictions of the NRM theory for mixtures and pure components. Although the differences are small, a binary mixture and a pure component are predicted to behave differently. For small values of the interaction parameter $\langle e \rangle$, i.e. at low values of the site fraction ϕ_B, the mixture (—, ■) has a slightly smaller density than a pure component (– – –, ○) with the same interaction parameter. At higher concentrations of B, the density difference between mixtures and pure components is reversed. If one carefully inspects the simulation data for pure components and mixtures, a difference in density may be observed at high values for the effective interaction parameter $\langle e \rangle$. However, the simulation data have an uncertainty of the same order of magnitude as the observed differences. Hence, one should be careful in interpreting these differences in the simulation results. The accuracy of the MC simulation data can be appreciated from the two data points obtained for the pure component A ($\langle e \rangle = 0.5$) in Figure 1, which are the result of independent simulation runs (different starting configurations and different computers).

In Figure 2, using the same interaction constants as in Figure 1, the different contacts of component A in the blend according to simulation and NRM theory are shown (the random theory results are not presented in view of the qualitative results for the total density observed in Figure 1). In this figure, the covalent contacts of segments are excluded and the total number of other contacts of any A segment adds up to

$$(AA) + (AB) + (Ah) = z(1 - \alpha_A) = 4.066667 \quad (25)$$

A similar constraint is valid for the contacts viewed from a B segment. Due to the symmetry of the mixture ($e_{AA} = e_{BB}$ and $s_A = s_B$), the contacts of component B at composition ϕ_B, collected in the simulations in the interval ($0 < \phi_B < 0.5$), can be interpreted as the contacts of A segments at a composition ($1 - \phi_B$). Therefore, the collected simulation data are used to present the A contacts spanning the complete composition range. Through symmetry, the contacts of B can be read from Figure 2, if the following correspondences are applied: $\phi_B \rightarrow \phi_A$, (AA) → (BB), (AB) → (BA), and (Ah) → (Bh).

In Figure 2 the agreement between theory and simulation appears to be excellent. It should be noted that no fitting of theory to MC data is done: the theory is only used to predict. The contacts of A with vacancies

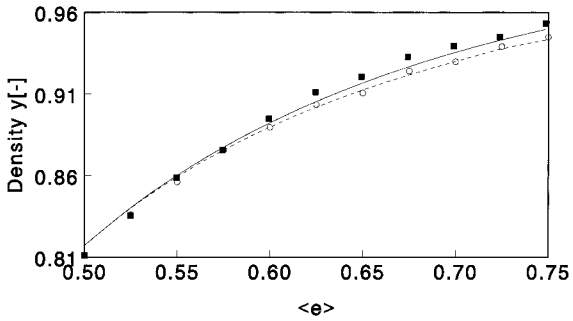

Figure 3. Density y as a function of the effective interaction parameter $\langle e \rangle$ for ($e_{AA} = e_{BB} = 0.5$) and varying e_{AB} ($0.5 \leq e_{AB} \leq 1$). Pure component results (○) and mixtures (■). Lines are predictions according to NRM theory: pure component (– – –) and mixtures (—).

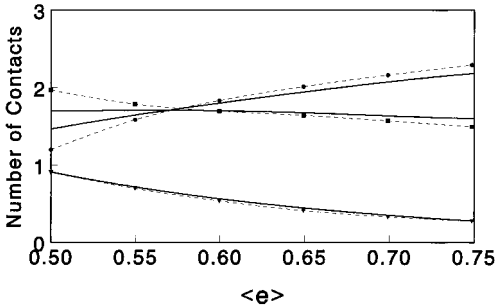

Figure 4. Number of different type of contacts of A segments as a function of effective interaction parameter $\langle e \rangle$ for the parameters used in Figure 3: AA contacts (■), AB contacts (●), and Ah contacts (▼). Full lines are predictions according to NRM theory. Dashed lines are splines to guide the eye.

(▼) are accurately predicted at all compositions. According to theory, the number of (AA) contacts (■) decreases to zero at $\phi_B = 1$. The simulations appear to indicate a leveling at high ϕ_B. It will be shown in later simulation sets (see Figures 4, 5, 8, and 9) that this discrepancy is due to the chain connectivity. The number of (AB) contacts (●), which have a purely intermolecular origin, start at zero in pure A, steadily increasing with ϕ_B.

The second set of simulation data is done for the same values of pure component parameters ($e_{AA} = e_{BB} = 0.5$) as a function of the value of the cross-interaction parameter e_{AB} ($0.5 \leq e_{AB} \leq 1.0$) at constant composition. The almost symmetric mixture composition $\phi_B = 0.48$ is selected to minimize possible effects of the chain connectivity of both components. It is often assumed that for this composition both components experience a practically homogeneous segment density, and a theory making use of a homogeneous segment density should be at its best. In Figure 3 it is clear that the concept of representing a mixture by its equivalent effective component breaks down with increasing asymmetry of the cross-interaction parameter e_{AB}. Both simulation and theory reveal a higher density of the mixtures (—, ■) compared to the effective single component (– – –, ○), although the NRM theory slightly underestimates the effect.

Also the microscopic details in the blend obtained from the different types of contacts in the blends are predicted satisfactorily (see Figures 4 and 5 for contacts made by A and B segments, respectively). Again the segment hole contacts are predicted accurately for all values of $\langle e \rangle$. The contacts involving segments only are accurately predicted if the results at $\langle e \rangle = 0.5$ are not taken into account. This may come as a surprise

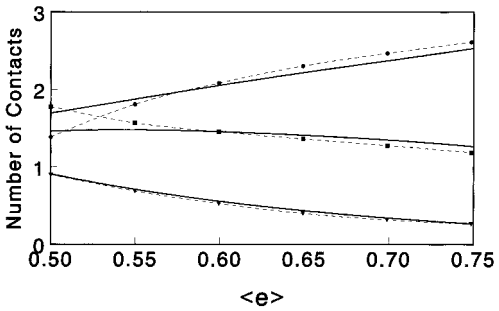

Figure 5. Number of different type of contacts of B segments as a function of effective interaction parameter $\langle e \rangle$ for the parameters used in Figure 3: BB contacts (■), BA contacts (●), and Bh contacts (▼). Full lines are predictions according to NRM theory. Dashed lines are splines to guide the eye.

because this mixture is the most ideal one of all mixtures considered in Figures 4 and 5. One may argue that the mean field theory, with a homogeneous segment density, should predict this particular case even better than the other mixtures. However, it is in this situation that the effect of chain connectivity becomes apparent, since the chains are effectively ideal and the contacts are not influenced by differences in interactions. Hence A segments will be preferentially surrounded by A segments, in comparison with the mean field value, due to chain connectivity. Contacts with B segments will not be as numerous (see Figure 4). The same applies to the contacts of B segments that favor BB contacts (see Figure 5). As these connectivity effects are not properly accounted for in the mean field theory (only the nearest-neighbor covalent bonds are considered in the NRM theory), the theory provides un underestimation of the (AA)/(BB) contacts (■) and hence an overestimation of the (AB)/(BA) contact numbers (●). Increasing the value of $\langle e \rangle$, making the cross-interactions more favorable, intermolecular contacts with the other component are favored and the effect of connectivity diminishes. An extra but small effect on contacts is the expansion of A and B chains, with respect to the ideal chain behavior, which was shown by Cifra, Karasz, and MacKnight in the case of favorable interactions.[40,41] This coil expansion results in an extra reduction of the intramolecular contacts, making the theoretical assumption better. The influence of the interactions on the formation of the intermolecular contacts is accounted for in the NRM theory. Although the precise origin (inter or intramolecular) of the (AA)/(BB) contact types is not predicted by the NRM theory, the agreement of simulation and theory indicates that the microscopic parameters $\bar{X}_{AB}$, $\bar{X}_{Bh}$, and $\bar{X}_{Ah}$ successfully incorporate the effects of the interactions on the partition function. However, it is to be expected that the theory will be less successful for asymmetric mixture compositions. Making implicit use of a homogeneous segment density, it should be anticipated that the theory will fail if the concentrations of one of the components becomes sufficiently dilute to have effectively isolated coils of this component in the mixture. In such situations, the microscopic parameters $\bar{X}_{AB}$, $\bar{X}_{Bh}$, and $\bar{X}_{Ah}$ will not suffice to accurately predict these effects due to chain connectivity.

In the next two sets of simulation data, the influence of composition and the asymmetry of pure component interaction parameters is investigated. In both sets the contact energy of component A, e_{AA}, is set to 0.5, and the value of e_{BB} is set to 0.7 and 0.9. The cross-interaction parameter is adjusted such that the Flory–Huggins exchange energy parameter $\Delta w = -(2\epsilon_{AB} - \epsilon_{AA} - \epsilon_{BB})$ equals zero. In the spirit of incompressible lattice theories, the exchange of pure component contacts for cross-contacts occurs without a change in Δw, and this is also the only energy parameter characterizing the mixture.[31] Of course, in the compressible theories investigated here, the exchange energy is not the only energy scale entering the discussion; the pure component parameters as such also influence the mixture properties.

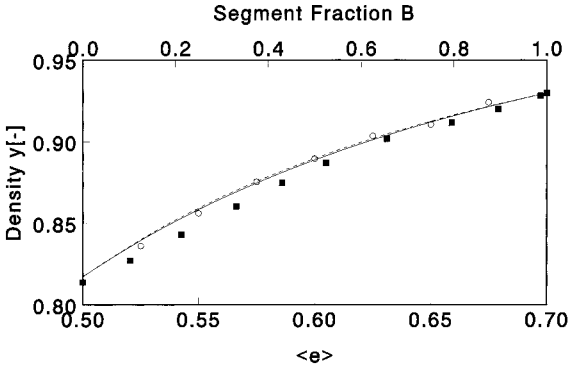

Figure 6. Density y as a function of the effective interaction parameter $\langle e \rangle$ (bottom axis) or of composition ϕ_B (top axis) for ($e_{AA} = 0.5$, $e_{BB} = 0.7$, $e_{AB} = 0.6$). Pure component results (○) and mixtures (■). Lines are predictions according to NRM theory: pure component (– – –) and mixtures (—).

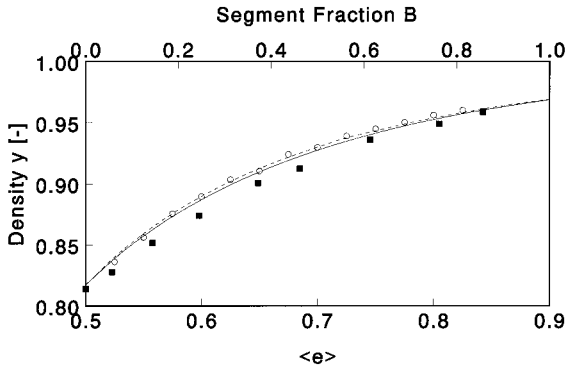

Figure 7. Density y as a function of the effective interaction parameter $\langle e \rangle$ (bottom axis) or of composition ϕ_B (top axis) for ($e_{AA} = 0.5$, $e_{BB} = 0.9$, $e_{AB} = 0.7$). Pure component results (○) and mixtures (■). Lines are predictions according to NRM theory: pure component (– – –) and mixtures (—).

The density as a function of composition or effective interaction parameter is shown in Figure 6 ($e_{BB} = 0.7$) and Figure 7 ($e_{BB} = 0.9$). In both figures the pure component results in the same interactional parameter as the effective interaction parameter are shown for comparison. Comparing simulation data, it is clear that the principle of an effective component is not valid and that the deviations increase with the asymmetry in pure component parameters. One can conclude that the principle of an effective component works in miscible blends, i.e. $\Delta w < 0$, as shown in Figure 1. In contrast, the effective component principle fails for mixtures, shown in Figures 6 and 7, in which the components have different interaction constants and $\Delta w = 0$. In the NRM theory, mixtures (—) and pure components (– – –) also behave differently, but the difference is not as pronounced as in the simulation. However, a density decrease upon mixing is predicted, in agreement with simulation. Additional interesting information is obtained from the different types of contacts. In Figure 8 the contacts of B segments are shown as a function of composition and effective interaction parameter for the

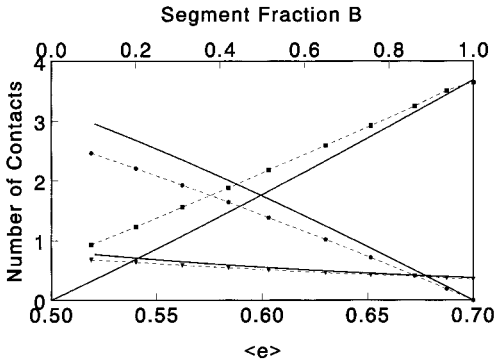

Figure 8. Number of different type of contacts of B segments as a function of effective interaction parameter $\langle e \rangle$ (bottom axis) or composition (top axis) for the parameters used in Figure 6: BB contacts (■), BA contacts (●), and Bh contacts (▼). Full lines are predictions according to NRM theory. Dashed lines are splines to guide the eye.

simulation set shown in Figure 6. The number of segment vacancy contacts (▼) are accurately predicted over the whole composition and/or interaction range. However, (BB) contacts and (BA) contacts show deviations with varying composition. For the (BB) contacts (■) the number of contacts is predicted well at small concentrations of component A, but the predictions deteriorate with increasing A content. The mean field result approaches zero in pure A, as expected, whereas the simulation results show a finite number of (BB) contacts. These remaining contacts are of intramolecular origin due to chain connectivity. For the number of (BA) contacts (●) a similar observation is made. In pure B both theory and simulation show no heterocontacts, whereas approaching pure A, too many contacts are predicted. The reason for these differences has already been addressed in the discussion of Figures 4 and 5 and alluded to in Figure 2. Due to chain connectivity, B segments experience more B contacts, relative to the overall blend composition, than predicted in the mean field theory. Taking into account the constraint, eq 25, the (BA) contacts are overpredicted. Similar reasoning applies to the contacts made viewed from an A segment, but is not repeated here.

The deficiencies of the mean field theories (including the NRM theory), assuming a homogeneous segment density, can be clearly exposed in the case of athermal mixtures ($e_{AA} = e_{BB} = e_{AB} = 0$). In the case of equal chain lengths, which is discussed in this paper ($s_A = s_B = s = 30$), the equation of state is truly independent of composition (A and B are indistinguishable) and identical to that of a single component with the same chain length. The densities at three different pressures are $y(10 \text{ bar}) = 0.278$, $y(20 \text{ bar}) = 0.382$, and $y(40 \text{ bar}) = 0.505$. It was shown in an earlier paper that the athermal EoS is predicted quite well for the chain lengths considered here.[10] However, a detailed comparison of the different contacts in the mixture clearly shows the deficiencies of the theories. In Figure 9 the different types of contacts of A segments are shown as a function of the mixture composition, expressed in ϕ_B at 40 bar (in this comparison, the covalent contacts are again explicitly excluded). The number of contacts involving vacancies (▼) is predicted quite accurately, in agreement with the quality of prediction of overall density. However, the situation is different for the contacts involving other segments. For instance, the number of (AA) contacts (■) is predicted to decrease with ϕ_B and in pure B the conditional number of (AA) contacts equals zero. However, the simulation shows

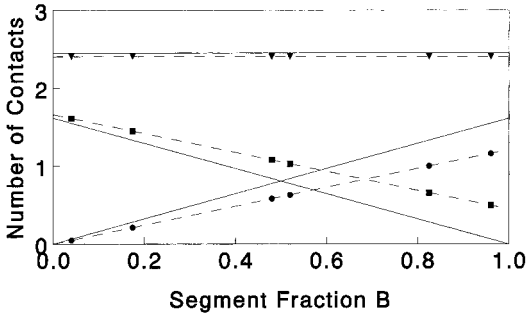

Figure 9. Number of different type of contacts of A segments as a function of composition for athermal mixtures ($e_{AA} = e_{BB} = e_{AB} = 0$) at $p = 40$ bar: AA contacts (■), AB contacts (●), and Ah contacts (▼). Full lines are predictions according to NRM theory. Dashed lines are splines to guide the eye.

a decrease in (AA) contacts to a limiting value at $\phi_B = 1$, which is due to the chain connectivity. Even at infinite dilution, A segments remain surrounded by intramolecular A segments that result in a nonzero number of (AA) contacts in pure B. The number of (AB) contacts (●), starting in pure A from zero, is predicted to increase with ϕ_B. The simulation shows the same limiting behavior since (AB) contacts only involve intermolecular contacts that vanish if one of the components is infinitely diluted. The value of (AB) contacts with increasing ϕ_B is overestimated, which is a direct consequence of the inaccurate limiting behavior of the (AA) contacts and the constraint on the total number of contacts a segment can make, given by eq 25. Figure 9 applies equally well to B contacts if the following changes are made: $\phi_B \rightarrow \phi_A$, (AA) → (BB), (AB) → (BA), and (Ah) → (Bh). From this comparison, it is clear that the assumption of a homogeneous segment distribution is not really fulfilled. Even in the symmetric blend ($\phi_B = 0.5$), theoretical and simulated numbers of contacts deviate significantly. It is only in the pure component that differences between inter- and intramolecular contacts are effectively screened.

Sariban and Binder also presented a comparison of the different type of contacts in a ternary mixtures of two chainlike components and a constant fraction of vacancies on a lattice. In their comparison, they distinguished between inter- and intramolecular (AA)/(BB) contacts. In our comparison, no explicit distinction is made between intra- and intermolecular self-contacts. If one is only interested in the EoS of the mixture, this is not strictly necessary as the overall densities of the mixtures are predicted satisfactorily by the use of the microscopic parameters $\bar{X}_{Ah}$, $\bar{X}_{Bh}$, and $\bar{X}_{AB}$, which successfully incorporate the influence of interactions on the number of contacts. Of course, deviations from the assumed homogeneous segment distribution become noticeable in cases where these intramolecular contacts play a significant role, i.e. when interactions are not governing the contacts made and for asymmetric compositions. Generally speaking, the equation of state is not very sensitive to the difference between the intramolecular of intermolecular self-contacts. The situation is different in the case of e.g. the liquid−liquid coexistence to be considered next.

4.2. Liquid−Liquid Coexistence. In a final set of simulations, the L−L coexistence is investigated for binary mixtures in which the components have identical EoS characteristics (i.e. identical interactional constants). Having the same EoS behavior, the mixtures can only show UCST phase behavior induced by an unfavorable enthalpy of mixing. The L−L coexistence

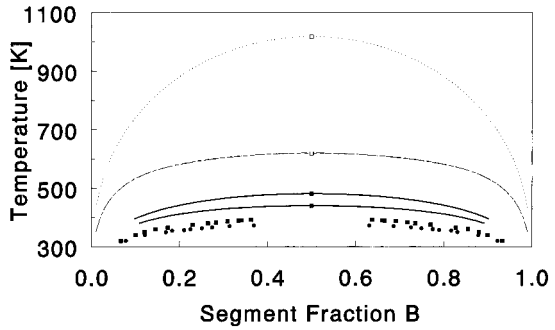

Figure 10. Binodal temperature as a function of composition at $p = 0$ bar (●) and $p = 30$ bar (■). The lines and (□) represent predictions of binodal and critical conditions for different theories. SFH theory (···), density-corrected SFH (−·−), LF theory (−−−), and NRM theory (—). Only for the NRM theory are predictions shown for the two pressures.

represents a very stringent test of the theory as it is governed by the subtle coexistence conditions (eq 14). In addition, the critical state is determined by the second and third compositional derivatives of the free enthalpy (eq 15). The binodal conditions have been investigated as a function of pressure. In Figure 10 the coexistence data for $p = 0$ and $p = 30$ bar are summarized together with results from different theories. Although it is possible to present these data in reduced units, they are shown in real thermodynamic variables temperature and pressure to make easier contact with experimental studies. As a reference, the frequently used simple SFH theory is shown (···). Note that this theory ignores the effects of compressibility (no vacancies are allowed on the lattice) and clearly this leads to too high a predicted UCST temperature ($T_C \sim 1100$ K). This can be understood as a simple consequence of the missing vacancies. The vacancies effectively dilute the unfavorable interactions that lead to the UCST phase behavior. Furthermore, the binodal curve is clearly too narrow compared to the simulation data. This has been observed very frequently, in comparisons of the SFH theory to experimental data, especially for polymer solutions. For such solutions this can be attributed, at least to a large extent, to the neglect of the covalent bonds in the evaluation of the internal energy.[42] Properly taking into account these covalent bonds leads to an extra composition dependence of the Flory−Huggins parameter, which results in a significant broadening of the miscibility gap. In this particular symmetric mixture, both components have the same number of covalent bonds and the extra compositional influence is not active (see eqs 23 and 24c) and does not result in an extra broadening. On the other hand, the LF theory (−−−) incorporates the compressibility effects and the prediction improves considerably. The UCST critical temperature is lowered drastically ($T_c \sim 630$ K) and the binodal curve is significantly broader. It should be noted that the LF theory does not account for the covalent bonds in energy and entropy either. Thus, it must be concluded that the compressibility effects not only lower the critical temperature but also influence the broadness of the miscibility gap. This is practically always ignored in the discussion of the UCST phase behavior, but this is apparently not justified.

At this point, it is worth mentioning the results of Sariban and Binder.[25−27] They showed that the critical temperature and coexistence curve at constant vacancy fraction could be obtained from the coexistence curve at full occupancy, by simply correcting the binodal temperature with the density according to

$$T_{\text{binodal}}(y\neq 1) = y_{\text{binodal}} \cdot T_{\text{binodal}}(y=1) \qquad (26)$$

The drastic decrease of the critical temperature according to the LF theory is indeed practically accounted for by the density on the lattice. In the compressible theory the density varies along the binodal as explicitly shown in Figure 12. Correcting the binodal temperature, obtained from the incompressible theory, for this vacancy fraction if accordance with eq 26, a curve (−·−) practically indistinguishable from the LF binodal curve is obtained. It should be noted that eq 26 cannot be true in general, as it is known that the compressibility effect has an extra destabilizing effect on the miscibility behavior. In this particular symmetric system, this extra destabilizing contribution is very small and practically not noticeable in Figure 10.

Finally, the NRM theory prediction, although approximately 60 K too high, is by far the best prediction along the theoretical approximations. The introduction of the NRM effects does not introduce any significant extra broadening of the binodal curve. The binodal curve is merely shifted closer to the MC simulation data. Compared to the LF theory, which results in an effective dilution of the unfavorable cross-contacts by the density y, the NRM theory, by virtue of the microscopic parameters $\bar{X}_{AB}$, $\bar{X}_{Ah}$, and $\bar{X}_{Bh}$, leads to a further efficient reduction of the cross-contacts in favor of the self-contacts. The predicted binodals are still too high in temperature, which, certainly in part, is due to the long-range connectivity of the chains not taken into account in the theory. In previous figures, it was shown that neglect of this chain connectivity resulted in an overestimation of the number of cross-contacts in the theory. It is clear that a further reduction in the cross-contacts by the chain connectivity, which carry an unfavorable energy, would lead to a lowering of the theoretical miscibility gap, thus closer to the simulations.

Although the pressure dependence is slightly overestimated, the agreement is satisfactory. The elevated pressure sensitivity is directly tied to the mismatch in cloud-point temperatures. At this high temperature, the lower density (see Figure 12, predictions according to the NRM theory (−−−)) results in a high compressibility, which in turn leads to the high-pressure sensitivity.

It is interesting to use the theory now, as it is used in most situations, and treat the MC simulation results as experimental data. As an illustration, the simulation data at zero pressure are used to estimate (some) parameters in the NRM theory. The most logical choice in the present situation is to fix the EoS properties (i.e. keep ϵ_{AA} and ϵ_{BB} at their correct values) and estimate the cross-parameter ϵ_{AB} from the MC experiments, especially from the 0 bar UCST critical temperature (this procedure results in a value for $\epsilon_{AB}/k = 191.70$ K). This will locate the binodal curve on the temperature scale, and with this estimated parameter, one can predict the rest of the binodal at 0 bar and predict critical conditions and binodals at other pressures. As can be seen in Figure 11 (an extra simulation set at $p = 10$ bar is incorporated), the predicted pressure dependence is in almost quantitative agreement with the simulation results. Here too the binodal curves remain slightly too narrow. This is, possibly, related to the inhomogeneous segment density that is especially pronounced at the sides of the phase diagram. It has been shown theoretically that the inhomogeneous segment distribution in polymer solutions[43,44] and blends[45]

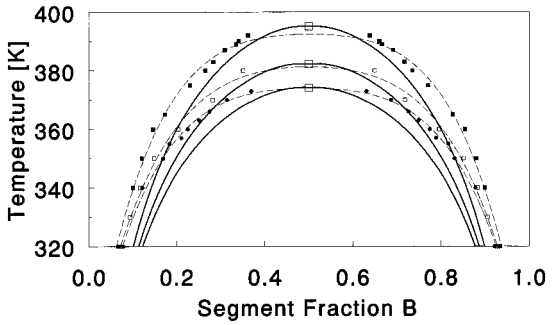

Figure 11. Binodal temperature as a function of composition at $p = 0$ bar (●), $p = 10$ bar (○), and $p = 30$ bar (■) (the dashed lines are splines to guide the eye). The full lines and (□) represent binodal curves and critical conditions predicted using the theoretical values of ϵ_{AA} and ϵ_{BB} and an estimate of the cross parameter ϵ_{AB} from the $p = 0$ bar critical temperature.

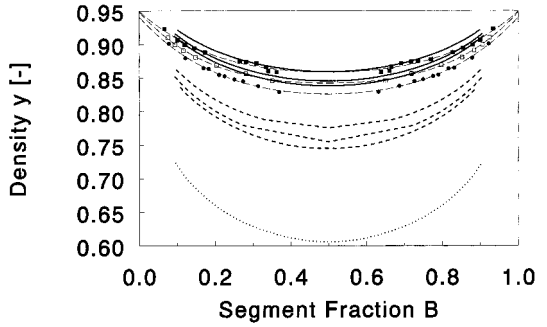

Figure 12. Density along the coexistence curves, shown in Figure 11, as a function of composition at $p = 0$ bar (●), $p = 10$ bar (▼), and $p = 30$ bar (■) (thin dashed lines are splines to guide the eye). The thick lines represent predictions according to LF theory (···), the NRM theory (– – –) and the adjusted NRM theory (—). For the LF theory only the $p = 0$ bar result is shown.

can result in a broadening of the miscibility gap. The shape of the coexistence curve in the vicinity of the consolute state is also affected by the critical behavior. For the short chain lengths discussed in this work, Sariban and Binder[39] showed that the coexistence curve in the critical region has not the parabolic shape predicted by mean field theories but is considerably flatter. This flatness is characterized by the Ising model critical exponent $\beta = 0.325$ in contrast to the mean field value $\beta = 0.5$ that leads to the parabolic behavior. The flattened critical region, in turn, also leads to a broadening of the coexistence curve.

In Figure 12 the density along the binodal curve is shown at different pressures. The MC data are compared with the theoretical results according to the LF theory (···), the prediction according to the NRM theory (– – –), and finally the results according to the adjusted NRM results (—). As the predicted binodal temperatures in the LF and NRM theories were too high, the predicted densities along the binodal curve are too low. On the other hand, the adjusted NRM theory gives a density that is slightly too high along the binodals, which is caused by the more favorable value of the adjusted cross-interactional parameter.

Microscopic information about the mean square end-to-end distance of both components along the binodal curve at $p = 0$ bar is presented in Figure 13. For asymmetric compositions, the minority chains have smaller dimensions. This was already shown by Sariban and Binder for a single composition and various interactions. The situation at the binodal is completely opposite to that of a miscible mixture. As shown by

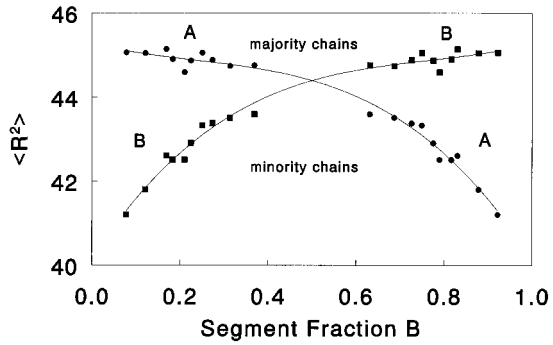

Figure 13. Mean square end-to-end distance $\langle R^2 \rangle$ of component A (●) and B (■) along the coexistence curve at $p = 0$ bar, shown in Figure 11, as a function of the composition of the coexisting phase.

Cifra, Karasz, and MacKnight, in compressible[40] as well as incompressible[41] systems, the minority component at asymmetric compositions expands due to the favorable environment provided by the other component. The majority component does not significantly change coil dimension and practically behaves as in its own melt.

5. Conclusion and Future Work

Thermodynamic and microscopic information for binary mixtures of compressible lattice chain molecules has been obtained, as a function of composition and a variety of the three interactional constants necessary to completely specify the interactions. A series of MC simulations were performed using the NpT and semigrand μpT ensembles. In all the cases discussed, the chain lengths of both components were taken to be equal, $s_A = s_B = 30$. The EoS was investigated as a function of composition and the interactional constants were varied to provide different values of the overall exchange energy $\Delta w = -(2\epsilon_{AB} - \epsilon_{AA} - \epsilon_{BB})$, which is the only energy scale entering the theory of the incompressible lattice model. For the liquid−liquid coexistence, an additional symmetry on the self-interactional constants ($\epsilon_{AA} = \epsilon_{BB}$) is imposed. For the first time, the coexistence of compressible lattice polymer mixtures was investigated as a function of pressure. Furthermore, microscopic data on the different type of contacts and the coil dimensions were obtained.

These MC simulation data were used to check theoretical predictions of the nonrandom mixing theory for binary compressible mixtures, which is analogous to the quasi-chemical approximation of Guggenheim for binary incompressible mixtures. The relation of this theory to other theoretical approximations for the compressible lattice model is explained.

Mean field theories working with a random mixing approximation make is possible to define a principle of a so-called effective component. Strictly speaking, this principle is not valid. However, it is closely approximated in mixtures with negative exchange energies Δw. Mixtures with Δw small or zero show increasing deviations from the effective component principle with increasing asymmetry in the pure component interaction energy parameters. The deficiencies of theories operating with a homogeneous density assumption become clear in the prediction of the different type of contacts. In such theories, the number of intramolecular self-contacts, due to the chain connectivity, are ignored, which results in an underestimation of the total number of self-contacts and an accompanying overestimation of the cross-contacts. The number of segment vacancy

contacts are predicted very accurately in all cases. Notwithstanding the clear drawback of these theories, the EoS turns out to be quite insensitive to the distinction in inter- and intramolecular self-contacts.

Taking the simple incompressible SFH lattice theory as a reference, it is shown that the simple introduction of vacancies leads to a dramatic lowering of the binodal temperature and a considerable broadening of the miscibility gap. This observation is in agreement with the results obtained by Sariban and Binder for ternary mixtures of two chain components and a fixed fraction of vacancies. The compressibility, due to the vacancies, not only determines the LCST phase behavior but is also important for the detailed appearance of the UCST phase behavior. In many theoretical considerations this is ignored in effect. The NRM theory that accounts for the interactional effects on energy and entropy leads to a further efficient reduction of the binodal temperature, due to a preference for self-contacts over cross-contacts, which are more favorable in the region of partial miscibility of the phase diagram. Nevertheless, important differences between theory and simulation remain. A factor certainly contributing to this is the theoretical neglect of the difference between intra- and intermolecular self-contacts. A further reduction of the binodal temperature can be anticipated if the influence of the preferential formation of self-contacts over cross-contacts by chain connectivity is accounted for. This effect, playing a role over the whole composition range is particularly important at the extreme composition sides of diagram. The distinction between intra- and intermolecular self-contacts also influences the EoS of homogeneous mixtures. It was shown that the presence of intra- and intermolecular self-contacts has some impact in mixtures for which the exchange energy parameter Δw is zero or positive. If Δw is negative, the microscopic parameters in the NRM theory correctly predict the variation in self- and cross-contacts.

In future work, the thermodynamic and microscopic properties of binary compressible mixtures will be further investigated. Possible extensions for symmetric mixtures include variations in chain length and a further variation in the values of the self-interactional constants. A further extension to more complicated systems will involve asymmetries in chain lengths and interactional constants. A substantial enrichment of the phase behavior will occur, and it will be of interest to systematically explore these asymmetries in the simulations as well as in the NRM theory.

From the theoretical point of view, the influence of chain connectivity will be investigated. Possible routes to include the nonhomogeneous segment density in chain molecular mixtures will be explored. It is clear, in view of the results obtained here, that efforts along these lines should include the influence of nonrandom mixing effects. The quantitative success of theoretical predictions is greatly determined by the latter.

References and Notes

(1) Staverman, A. J.; van Santen, J. H. *Recl. Trav. Chim. Pays-Bas* **1941**, *60*, 76.
(2) Staverman, A. J. *Recl. Trav. Chim. Pays-Bas* **1941**, *60*, 640.
(3) Flory, P. J. *J. Chem. Phys.* **1941**, *9*, 660.
(4) Flory, P. J. *J. Chem. Phys.* **1942**, *10*, 51.
(5) Huggins, M. L. *J. Chem. Phys.* **1942**, *43*, 1.
(6) Huggins, M. L. *Ann. N.Y. Acad. Sci.* **1942**, *43*, 1.
(7) Lacombe, R. H.; Sanchez, I. C. *J. Phys. Chem.* **1976**, *80*, 2568.
(8) Sanchez, I. C.; Lacombe, R. H. *J. Phys. Chem.* **1976**, *80*, 2352.
(9) Kleintjens, L. A.; Koningsveld, R. *Colloid Polym. Sci.* **1980**, *258*, 711.
(10) Nies, E.; Cifra, P. *Macromolecules* **1994**, *27*, 6033.
(11) Hansen, J. P.; McDonald, I. R. *Simple Theory of Liquids*, 2nd ed.; Academic Press: London, UK, 1986.
(12) Binder, K. *Annu. Rev. Phys. Chem.* **1992**, *43*, 33.
(13) Dickman, R.; Hall, C. K. *J. Chem. Phys.* **1986**, *85*, 4108.
(14) Dickman, R.; Hall, C. K. *J. Chem. Phys.* **1988**, *89*, 3168.
(15) Honnell, K. G.; Hall, C. K. *J. Chem. Phys.* **1988**, *90*, 1841.
(16) Yethiraj, A.; Hall, C. K. *J. Chem. Phys.* **1991**, *95*, 8494.
(17) Lennard-Jones, J. E.; Devonshire, A. F. *Proc. R. Soc. London, A* **1937**, *163*, 63.
(18) Prigogine, I.; Bellemans, A.; Mathot, V. *The Molecular Theory of Solutions*; North-Holland Publishing Co.: Amsterdam, 1957.
(19) Simha, R.; Somcynsky, T. *Macromolecules* **1969**, *2*, 341.
(20) Simha, R.; Carri, G. *J. Polym. Sci, Polym. Phys. Ed.* **1994**, *32*, 2645.
(21) Nies, E.; Stroeks, A. *Macromolecules* **1990**, *23*, 4092.
(22) Nies, E.; Xie, H. *Macromolecules* **1993**, *26*, 1683.
(23) Stroeks, A.; Nies, E. *Macromolecules* **1990**, *23*, 4088.
(24) Xie, H.; Nies, E. *Macromolecules* **1993**, *26*, 1689.
(25) Sariban, A.; Binder, K. *Macromolecules* **1988**, *21*, 711.
(26) Sariban, A.; Binder, K. *Makromol. Chem.* **1988**, *189*, 2537.
(27) Sariban, A.; Binder, K. *Colloid Polym. Sci.* **1988**, *266*, 389.
(28) Deutsch, H. P. *J. Chem. Phys.* **1993**, *99*, 4825.
(29) Mueller, M.; Binder, K. *Macromolecules* **1995**, *28*, 1825.
(30) Hertanto, A.; Dickman, R. *J. Chem. Phys.* **1988**, *89*, 3168.
(31) Madden, W. G.; Pesci, A. I.; Freed, K. F. *Macromolecules* **1990**, *23*, 1181.
(32) Carmesin, I.; Kremer, K. *Macromolecules* **1988**, *21*, 2819.
(33) Guggenheim, E. A. *Mixtures*; Oxford University Press: London, 1952.
(34) *The NAG Fortran Library Manual, Mark 15*; NAG Ltd.: Oxford, UK, 1991.
(35) Gibbs, J. *The Collected Works of J. Williard Gibbs*; Longmans, Green: London, UK, 1928−1931; Vol. 1.
(36) Cifra, P.; Bruder, F.; Brenn, R. *J. Chem. Phys.* **1993**, *99*, 4142.
(37) Panagiotopoulos, A. Z. *Mol. Simul.* **1992**, *9*, 1.
(38) Siepmann, J. I.; Frenkel, D. *Mol. Phys.* **1992**, *75*, 59.
(39) Sariban, A.; Binder, K. *J. Chem. Phys.* **1987**, *86*, 5859.
(40) Cifra, P.; Karasz, F. E.; MacKnight, W. J. *Macromolecules* **1992**, *25*, 4895.
(41) Cifra, P.; Karasz, F. E.; MacKnight, W. J. *Macromolecules* **1992**, *25*, 192.
(42) Nies, E.; Koningsveld, R.; Kleintjens, L. A. *Prog. Polym. Colloid Sci.* **1985**, *71*, 2.
(43) Koningsveld, R.; Stockmayer, W. H.; Kennedy, J. W.; Kleintjens, L. A. *Macromolecules* **1974**, *7*, 73.
(44) Muthukumar, M. *J. Chem. Phys.* **1986**, *85*, 4722.
(45) Bates, F. S.; Muthukumar, M.; Wignall, G. D.; Fetters, L. J. *J. Chem. Phys.* **1988**, *89*, 535.

MA960154S